Tissue-specific p19[superscript Arf] regulation dictates the response to oncogenic K-ras

Citation: Young, N. P., and T. Jacks. "Tissue-specific p19Arf regulation dictates the response to oncogenic K-ras." Proceedings of the National Academy of Sciences 107, no. 22 (June 1, 2010): 10184-10189.

As Published: http://dx.doi.org/10.1073/pnas.1004796107

Publisher: National Academy of Sciences (U.S.)

Persistent URL: http://hdl.handle.net/1721.1/84633

Version: Final published version: final published article, as it appeared in a journal, conference proceedings, or other formally published context

Tissue-specific $p19^{Arf}$ regulation dictates the response to oncogenic K-ras

Nathan P. Young[a] and Tyler Jacks[a,b,1]

[a]Koch Institute for Integrative Cancer Research and Department of Biology and [b]Howard Hughes Medical Institute, Massachusetts Institute of Technology, Cambridge, MA 02139

Contributed by Tyler Jacks, April 8, 2010 (sent for review February 27, 2010)

The ability of oncogenes to engage tumor suppressor pathways represents a key regulatory mechanism that can limit the outgrowth of incipient tumor cells. For example, in a number of settings oncogenic Ras strongly activates the *Ink4a/Arf* locus, resulting in cell cycle arrest or senescence. The capacity of different cell types to execute tumor suppressor programs following expression of endogenous K-ras^{G12D} in vivo has not been examined. Using compound mutant mice containing the Arf^{GFP} reporter and the spontaneously activating $K\text{-}ras^{LA2}$ allele, we have uncovered dramatic tissue specificity of K-ras^{G12D}-dependent $p19^{Arf}$ up-regulation. Lung tumors, which can arise in the presence of functional $p19^{Arf}$, rarely display $p19^{Arf}$ induction. In contrast, sarcomas always show robust activation, which correlates with genetic evidence, suggesting that loss of the $p19^{Arf}$-p53 pathway is a requisite event for sarcomagenesis. Using constitutive and inducible RNAi systems in vivo, we highlight cell type-specific chromatin regulation of *Ink4a/Arf* as a critical determinant of cellular responses to oncogenic K-ras. Polycomb-group complexes repress the locus in lung tumors, whereas the SWI/SNF family member Snf5 acts as an important mediator of $p19^{Arf}$ induction in sarcomas. This variation in tumor suppressor induction might explain the inherent differences between tissues in their sensitivity to Ras-mediated transformation.

tumor suppression | Ink4a/Arf | chromatin | BMI1 | SNF5

An emerging paradigm in cancer biology is the duality of oncogenic signaling. Through their ability to activate a number of progrowth and prosurvival pathways, oncogenes potently promote tumor initiation and progression. However, oncogenes also can engage tumor suppressor pathways, which results in a permanent cell cycle arrest (termed senescence) and/or cell death. These findings have led to the concepts of oncogene-induced senescence (OIS) and oncogene-induced apoptosis (OIA) as two crucial tumor suppressor checkpoints functioning to restrain tumor growth (1–3).

Two of the main mediators of these anti-oncogenic programs are encoded by the *Ink4a/Arf* locus, which contains two overlapping, but structurally distinct, tumor suppressors: $p19^{Arf}$ ($p14^{Arf}$ in humans) and $p16^{Ink4a}$. $p19^{Arf}$ is a nucleolar protein, the most well-established role of which is to indirectly activate the p53 transcription factor by interfering with the function of its inhibitor Mdm2. $p16^{Ink4a}$ functions as a cyclin-dependent kinase inhibitor that promotes cell cycle arrest by binding cyclin D/CDK4/6 complexes and preventing RB phosphorylation (4). In response to a variety of stresses, such as oncogenic Ras activation, these genes are coordinately up-regulated, which leads to p53 and Rb pathway activation and ultimate growth arrest (5–7). Therefore, Ink4a/Arf serves as a critical node linking upstream signals to downstream effector pathways during oncogene-induced tumor suppression.

Whether various cell types in distinct tissues have different inherent abilities to engage these programs following oncogenic insults remains largely unknown. Any such variability could have a profound influence on tumor susceptibility in different tissues and cell types, with cells responding by either proliferating as a result of low tumor suppressor induction or robustly up-regulating checkpoints and halting tumor initiation. Such a phenomenon could explain the tumor spectrum in the "latent" K-ras^{G12D} ($K\text{-}ras^{LA2}$) mouse model (8). In this model, an oncogenic allele of K-ras was engineered such that a duplication of exon 1 prevents its expression. Following a spontaneous recombination event, which in theory can occur in any cell type, the duplication is resolved and K-ras^{G12D} is expressed at endogenous levels. Despite the presumed random nature of oncogenic K-ras expression, these mice predominantly succumb to lung tumors; a subset also develops thymic lymphomas (8). The strong lung tumor phenotype could be due to the fact that certain lung cells that fail to effectively induce $p19^{Arf}$ and $p16^{Ink4a}$ are therefore sensitive to oncogenic K-ras–mediated transformation. In contrast, numerous other cell types in these animals could strongly activate Ink4a/Arf following K-ras^{G12D} expression, which would block tumor formation.

Previous studies have demonstrated that oncogene levels can determine whether a cell undergoes proliferation or cell cycle arrest/death. For example, although moderate signaling from Raf was shown to mediate cell cycle progression, increasing levels elicited cell cycle arrest (9). Additionally, alleles of oncogenic K-ras allowing for Cre-dependent expression of endogenous K-ras^{G12D} (e.g., $K\text{-}ras^{LSL\text{-}G12D}$) immortalized primary mouse embryonic fibroblasts, as opposed to inducing OIS, as was seen with retroviral-mediated over-expression of K-ras^{G12D} (10). This concept has also been validated in vivo (11, 12). Sarkisian et al. (11) have used doxycycline-inducible oncogenic H-ras to alter oncogene levels and shift the response from proliferation (low H-ras) to growth suppression (high H-ras). These data provide support for a model of oncogene levels dictating OIS or OIA versus proliferation in a given cell type and could also explain any different responses across tissues if oncogene levels varied accordingly.

An alternative explanation for variable Ink4a/Arf induction in response to oncogenic signaling underlies cell-type–specific locus regulation that sets different thresholds for gene expression. An increasing number of epigenetic regulators have been implicated in Ink4a/Arf activation and repression, presumably through their ability to confer upon the locus a particular chromatin confirmation and affect the accessibility of other transcription factors. Polycomb-group (PcG) proteins repress *Ink4a/Arf* in a number of cell types through direct binding of the histone methyltransferase containing Polycomb repressive complex 2 (PRC2) (including Ezh2 and Suz12) and the repressive PRC1 (including Bmi-1 and CBX8) (13–16). This mode of regulation seems to be especially important in multiple types of stem cells compared to their differentiated progeny (17). Recently, lineage-specific PcG regulation was proposed to explain the inherent differences in transformation capabilities of progenitor-like hematopoietic cells versus B and T cells (18, 19). In other systems, it is con-

Author contributions: N.P.Y. and T.J. designed research; N.P.Y. performed research; N.P.Y. contributed new reagents/analytic tools; N.P.Y. and T.J. analyzed data; and N.P.Y. and T.J. wrote the paper.

The authors declare no conflict of interest.

Freely available online through the PNAS open access option.

[1]To whom correspondence should be addressed. E-mail: tjacks@mit.edu.

This article contains supporting information online at www.pnas.org/lookup/suppl/doi:10.1073/pnas.1004796107/-/DCSupplemental.

ceivable that, across cell types with similar chromatin-bound PcG complexes, oncogene activation could result in cell-type–specific chromatin remodeling and Ink4a/Arf expression. For example, the proper up-regulation of PcG-repressed genes requires additional chromatin modifiers, including the SWI/SNF family of nucleosome remodelers (20, 21). This complex might have tissue-specific functions that allow it to exert influence over PcG regulation only in some settings. Overall, the balance between classes of epigenetic regulators could have a large influence on the ability of cells to engage the *Ink4a/Arf* locus in response to oncogenic signaling.

Here we report a tumor-type–dependent expression pattern of $p19^{Arf}$ in endogenous K-ras^{G12D}–driven lung tumors and sarcomas that correlates with the differential genetic requirements for tumor formation of these tissues. Although oncogene levels and signaling outputs appear similar between the tumors, we identify and functionally validate direct chromatin regulators as critical determinants of $p19^{Arf}$ expression. These findings suggest that tissue-specific chromatin remodeling can control tumor suppressor induction and provides a possible explanation for the different inherent sensitivities of distinct cell types to K-ras–mediated transformation.

Results

Deletion of $p19^{Arf}$ Expands the Tumor Spectrum of K-ras^{LA2} Mice. To monitor the activity of the $p19^{Arf}$-p53 pathway in vivo in the context of endogenous K-ras^{G12D} signaling, we crossed *K-ras*^{LA2} animals with the *Arf*^{GFP} reporter mouse (22). In this allele, GFP has been knocked into the endogenous $p19^{Arf}$ locus such that $p19^{Arf}$ function is abolished and GFP is under the control of the endogenous promoter. Thus, we could examine $p19^{Arf}$ promoter activity independently of any selective pressure to inactivate this locus during spontaneous tumor development in *K-ras*^{LA2} mice.

As shown in Fig. 1*A*, we noted a striking difference in median survival between *K-ras*^{LA2}*; Arf*$^{GFP/+}$ and *K-ras*^{LA2}*; Arf*$^{GFP/GFP}$ littermates. Upon close examination of aged *K-ras*^{LA2}*; Arf*$^{GFP/GFP}$ mice, it became evident that a number of animals had grossly detectable masses before death. Through histological examination, we determined that these masses represented two broad types of tumors not normally seen in *K-ras*^{LA2} animals. About 35% of mice had muscle-derived sarcomas that contained mostly spindle-shaped cells with varying degrees of differentiation. A quarter of compound mutant mice displayed enlarged spleens and livers that contained large cells with irregular nuclei and abundant cytoplasm, features reminiscent of histiocytic sarcomas (Fig. 1 *B* and *C*). Importantly, these tumors exhibited activated Ras, suggesting that they derived from cells in which the *K-ras*^{LA2} locus has recombined, similarly to the lung tumors found in *K-ras*^{LA2} mice (Fig. 1*D*). One interpretation of the expanded tumor spectrum in *K-ras*^{LA2}*; Arf*$^{GFP/GFP}$ mice is that there are cells in *K-ras*^{LA2}*; Arf*$^{+/+}$ animals that express oncogenic K-ras but fail to form tumors due to the strong induction of the $p19^{Arf}$-p53 pathway.

Variation in the Degree of Ink4a/Arf Activation Across Tumor Types in K-ras^{LA2}; $Arf^{GFP/GFP}$ Mice. We hypothesized that cells that give rise to tumors in *K-ras*^{LA2} mice only when $p19^{Arf}$ is deleted should have high levels of $p19^{Arf}$ expression upon K-ras^{G12D} activation. Indeed, comparing GFP induction across the various tumor types that form in *K-ras*^{LA2}*; Arf*$^{GFP/GFP}$ mice revealed dramatic differences in reporter induction (Fig. S1). The expression pattern was most striking and reproducible between lung tumors and muscle-derived sarcomas (hereafter referred to as sarcomas), with the sarcomas consistently expressing much higher levels of GFP than lung tumors (Fig. 2*A*). To extend these findings beyond the GFP reporter, we assessed levels of endogenous $p19^{Arf}$ protein in lung tumors and sarcomas from another mouse model in which we were able to control the timing and location of oncogenic K-ras activation. In the *K-ras*$^{LSL\text{-}G12D}$*; Trp53*$^{flox/flox}$ mouse model, lung tumors and sarcomas can be induced through administration of recombinant adenovirus expressing Cre recombinase (Ad-Cre) to either the lung or the muscle (23, 24). As shown in Fig. 2*B*, even though both tumor types developed in the absence of p53 and so might have been expected to both up-regulate $p19^{Arf}$ (25), steady-state levels of the protein were much higher in sarcomas than in lung tumors. Additionally, the expression pattern of $p16^{Ink4a}$, which shares its locus with $p19^{Arf}$ and is often coregulated, was identical to that of GFP (Fig. 2*C*). In summary, although

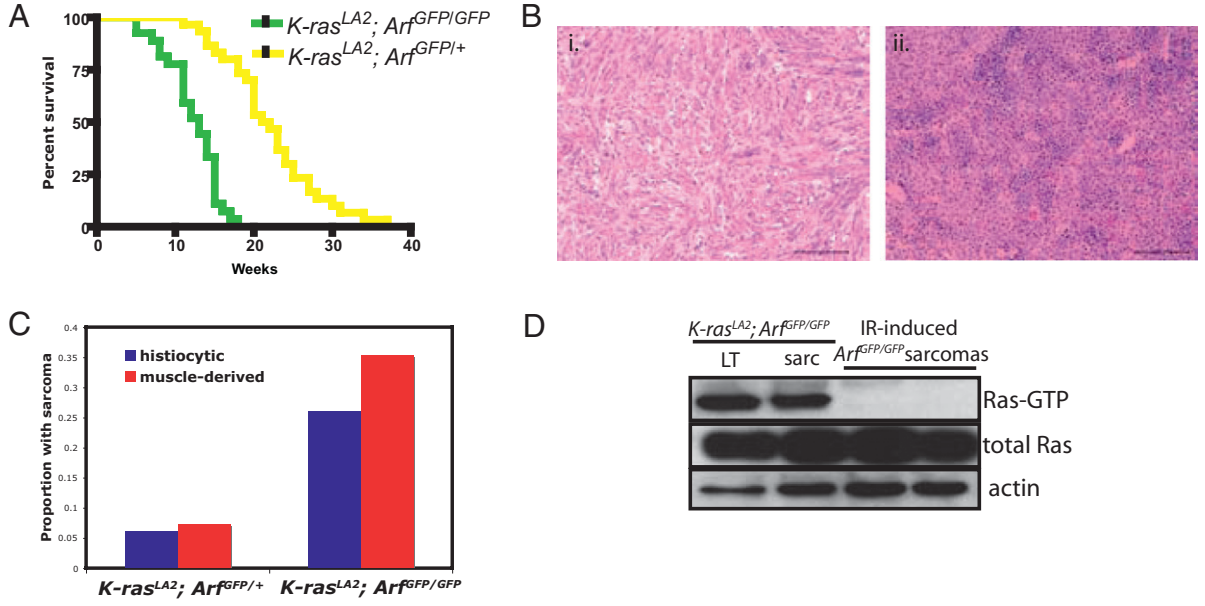

Fig. 1. Expanded tumor spectrum in *K-ras*^{LA2}*; Arf*$^{GFP/GFP}$ mice. (*A*) Kaplan–Meier survival plot of *K-ras*^{LA2}*; Arf*$^{GFP/+}$ ($n = 30$, yellow line) and *K-ras*^{LA2}*; Arf*$^{GFP/GFP}$ ($n = 27$, green line) mice ($P < 0.0001$, Student's *t* test). (*B*) Representative hematoxylin- and eosin-stained sections of sarcomas in *K-ras*^{LA2}*; Arf*$^{GFP/GFP}$ mice. (i) Muscle-derived sarcomas. (ii) Histiocytic sarcomas. (Scale bar: 100 μm.) (*C*) Percentage of *K-ras*^{LA2}*; Arf*$^{GFP/+}$ and *K-ras*^{LA2}*; Arf*$^{GFP/GFP}$ animals presenting with macroscopic muscle-derived sarcomas (red bars) or histiocytic sarcomas (blue bars). (*D*) Ras-GTP assay demonstrating activated Ras in muscle-derived sarcomas from *K-ras*^{LA2}*; Arf*$^{GFP/GFP}$ compound mutant mice. For a negative control, sarcomas induced by irradiation of *Arf*$^{GFP/GFP}$ mice do not show activated Ras.

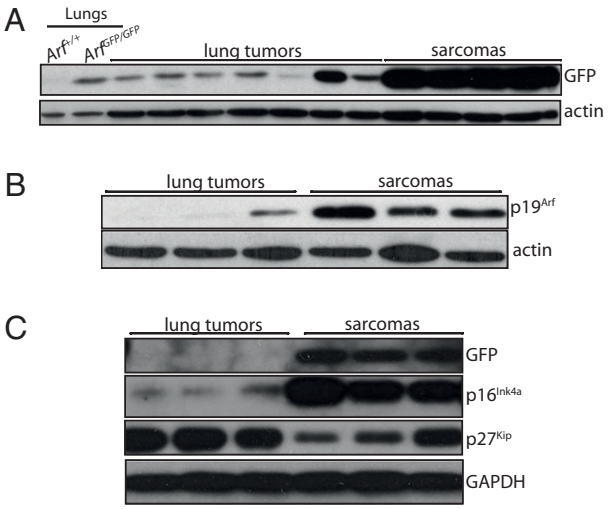

Fig. 2. Differential p19^{Arf} expression in K-ras^{G12D}-induced lung tumors and sarcomas. (*A*) GFP Western blots on lung tumors and muscle-derived sarcomas from *K-ras^{LA2}; Arf$^{GFP/GFP}$* mice. (*B*) Comparison of endogenous p19^{Arf} protein levels in lung tumors and sarcomas generated from Ade-Cre–infected *K-ras$^{LSL-G12D}$; Trp53$^{flox/flox}$* mice. (*C*) Western blots of GFP as well as tumor suppressor genes, p16^{Ink4a} and p27^{Kip1}, from lung tumors and sarcomas taken from *K-ras^{LA2}; Arf$^{GFP/GFP}$* mice. The pattern of lower tumor suppressor induction in lung tumors compared to sarcomas is specific to Ink4a/Arf, because p27, an unrelated tumor suppressor, shows the opposite correlation.

both tumors are driven by the same oncogene, sarcomas induce Ink4a/Arf much more strongly than do lung tumors.

Tissue-Specific p19^{Arf} Levels Correlate with Strength of Tumor Suppression. The absence of sarcomas in *K-ras^{LA2}* mice suggested that high levels of p19^{Arf} induction suppress tumor initiation in the muscle. To gain insight into this possibility, we again used the sarcoma model based on Ad-Cre delivery into the limbs of *K-ras$^{LSL-G12D}$; Trp53$^{flox/flox}$* mice. We have previously shown that sarcomas formed in this model only when both alleles of *Trp53* were inactivated (23). Substituting homozygous *Arf^{GFP}* alleles for *Trp53^{flox}* also supported sarcoma formation (Fig. S2). When leg muscles of both *Trp53$^{flox/+}$* and *Arf$^{GFP/+}$* (both *K-ras$^{LSL-G12D}$*) animals were subjected to systematic histological examination 4–7 months post Cre delivery, there were no preneoplastic lesions in the region of Ad-Cre delivery. This suggests that K-ras^{G12D} mutant cells are blocked early during tumor initiation, most likely because of rapid and robust p19^{Arf}-dependent tumor suppression.

In contrast, the moderate-to-low levels of p19^{Arf} present in lung tumors implied a weaker suppressive role for this locus. To test this, we assessed the functional consequences of *Arf* deletion on lung tumorigenesis. To this end, we generated cohorts of *K-ras^{LA2}* animals that were either *Arf$^{GFP/+}$* or *Arf$^{GFP/GFP}$* and compared tumor phenotypes at two different time points. Although tumor number was unaffected by *Arf* deficiency (Fig. S3*A*), at the later time point *K-ras^{LA2}; Arf$^{GFP/GFP}$* mice trended toward larger tumors that were more histologically advanced (Fig. S3 *B* and *C*). Importantly, similar results have been observed with *p53* mutations in the context of *K-ras$^{LSL-G12D}$*–driven lung tumors, in which *p53* deletion has no effect on tumor number but increases the size and grade of established tumors (26). These results suggest that disruption of the p19^{Arf}-p53 pathway primarily influences the progression of established lung tumors. Taken together, we conclude that the expression pattern of p19^{Arf} between lung tumors and sarcomas leads to dramatically different functional outputs of the p19^{Arf}-p53 pathway in cells expressing oncogenic K-ras in the two tissues.

Similar Oncogenic Signaling in Lung Tumors and Sarcomas. We next sought to understand the mechanistic basis of the tissue-specific expression pattern of p19^{Arf}. The regulation of p19^{Arf} expression is largely controlled by the intensity of signaling pathways downstream of oncogenic Ras, which are themselves directly regulated by overall oncogene levels (4, 10, 11, 27). Our initial hypothesis was that sarcomas have increased oncogenic signaling compared to lung tumors. Therefore, we analyzed steady-state levels of K-ras and some of the relevant downstream signaling outputs, including the Erk/MAPK, PI3K, and p38MAPK pathways, between lung tumors and sarcomas from *K-ras^{LA2}; Arf$^{GFP/GFP}$* mice. This analysis did not reveal any correlations between oncogene or signaling pathway levels and GFP induction across the two tumor types (Fig. S4). This suggests that the unique expression pattern of p19^{Arf}-GFP in lung tumors and sarcomas cannot be explained by differential levels of oncogenic signaling.

PcG Proteins Actively Repress Ink4a/Arf in Established Lung Tumors. Chromatin structure has a major influence on the ability of upstream signals to execute transcriptional programs at target loci. Therefore, we decided to monitor chromatin regulators as well as the chromatin composition of the *Ink4a/Arf* locus in lung tumors and sarcomas. Given their established role in *Ink4a/Arf* chromatin regulation in a number of settings, we began by investigating PcG proteins (13–16). Chromatin immunoprecipitation (ChIP) experiments revealed a striking difference in PcG occupancy at *Ink4a/Arf* between lung tumors and sarcomas from *K-ras^{LA2}; Arf$^{GFP/GFP}$* animals. Lung tumors consistently showed an enrichment of the PcG-associated histone mark, H3 Lys27 trimethylation (H3-K27me3), at the promoters of both p19^{Arf} and p16^{Ink4a} compared with sarcomas (Fig. 3*A* and Fig. S5*A*). In addition, binding of Bmi-1 was much more robust in lung tumors (Fig. 3*A* and Fig. S5*A*). These differences in PcG function between tumor types cannot be explained simply by expression differences of either Bmi-1 or the H3-K27 methyltransferase Ezh2 because quantitative reverse transcription PCR (qRT-PCR) analysis revealed similar levels of expression of these two genes (Fig. 3*B*). Overall, these data suggest there is lung-tumor–specific PcG-mediated gene silencing of *Ink4a/Arf*.

To functionally address whether PcG repressed p19^{Arf} in established lung tumors, we combined the *Arf^{GFP}* reporter with a unique system for inducible RNAi in vivo. We generated triple-mutant mice containing *Arf^{GFP}*, a recently constructed Flp recombinase-inducible K-ras^{G12D} allele (*K-ras$^{FSF-G12D}$*), and a widely expressed tamoxifen-inducible allele of Cre, *R26$^{CreER-T2}$* (28). To initiate tumors, bifunctional lentiviruses containing Flpo (29) were administered intratracheally into these mice. These viruses also contained a Cre-inducible shRNA cassette for expression of shRNAs to luciferase or Bmi-1. Twelve to 16 weeks after tumor initiation, shRNAs were induced by activating CreER via intraperitoneal injection with tamoxifen. One week later, lung tumors were harvested and analyzed for Bmi-1 knockdown and GFP expression (Fig. S5*B*). As shown in Fig. 3*C*, this system achieved reliable knockdown of Bmi-1 to levels about one-third of those observed in control hairpin tumors. Importantly, tumors with Bmi-1 knockdown displayed increased GFP levels compared to controls (Fig. 3*D*). p16^{Ink4a} was up-regulated as well (Fig. S5*C*). These data are consistent with a model in which PcG proteins function to maintain a closed chromatin state of *Ink4a/Arf* in lung tumors, leading to partial repression of p19^{Arf} and p16^{Ink4a}.

The SWI/SNF Family Member Snf5 Links K-ras^{G12D} Activation to p19^{Arf} Induction in Sarcomas. The presence of the PcG histone mark in sarcomas suggested that this chromatin-remodeling complex had some residual function at *Ink4a/Arf* in these tumors. Because PcG is known to repress this locus in a number of wild-type tissues, it is possible that the observed pattern reflected the activity of PcG in the cell-of-origin of the sarcomas. We hypothesized that, following

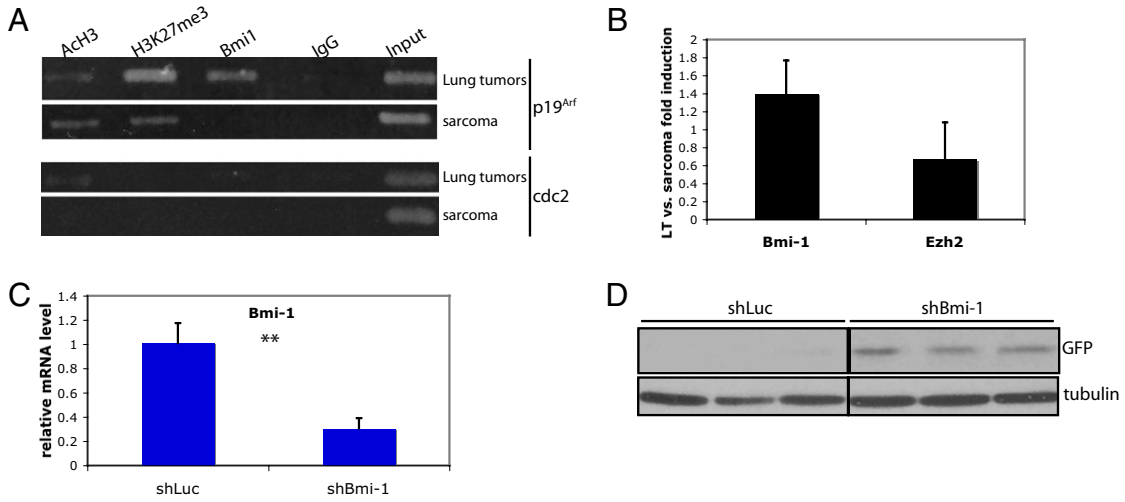

Fig. 3. PcG proteins repress the *Ink4a/Arf* locus in established lung tumors. (*A*) ChIP analysis of PcG markers in lung tumors and sarcomas from *K-ras*^{LA2}*; Arf*$^{GFP/GFP}$ mice. AcH3: acetylated histone H3, a mark of active transcription; H3-K27: trimethylated lysine 27 on histone H3, the PcG-associated chromatin mark. IgG corresponds to a control IP with rabbit IgG. Immunoprecipated as well as input DNA was amplified with primers specific to the promoters of p19^{Arf} and cdc2 (*B*) qRT–PCR of selected PRC2 (Ezh2) and PRC1 (Bmi-1) components in *K-ras*^{LA2}*; Arf*$^{GFP/GFP}$–derived tumors. The *y* axis is the fold induction of lung tumors versus sarcomas. $n = 3$ for each data point. $P > 0.05$, Student's *t* test. (*C*) qRT–PCR of Bmi-1 in *K-rasFSF-G12D; R26CreER-T2/CreER-T2; ArfGFP/GFP* lung tumors in which Luc (shLuc) ($n = 6$) or Bmi-1 (shBmi-1) ($n = 6$) shRNAs had been induced. (**$P < 0.0001$, Student's *t* test). (*D*) Western blot of GFP in shLuc and shBmi1 tumors. The two sides of the image are from the same exposure of the same blot, but the samples were not adjacent to each other. Error bars indicate SD.

K-ras^{G12D} expression, the locus might be remodeled such that PcG is mostly evicted and replaced by a distinct chromatin structure more conducive to gene activation. Studies in other model systems have implicated the SWI/SNF chromatin-remodeling complex as a critical player in this sort of antagonism of PcG-controlled gene repression (20, 21). Intriguingly, one member of SWI/SNF, Snf5, has recently been shown to directly bind and activate the *Ink4a/Arf* locus (30). Therefore, we investigated the requirement for Snf5 in the activation of p19^{Arf} in K-ras^{G12D}–driven sarcomas. Importantly, Snf5 was detectable by ChIP at *Ink4a/Arf* in multiple *K-ras*$^{LSL\text{-}G12D}$*; Arf*$^{GFP/GFP}$ cell lines derived from sarcomas (Fig. 4*A*). Furthermore, acute knockdown of Snf5 in these cell lines resulted in diminished GFP levels, suggesting a functional role for this chromatin modifier in p19^{Arf} regulation (Fig. 4*B*).

To test the significance of these findings in vivo, we first devised a functional assay using lentivirus-mediated RNAi in the muscle (Fig. S6). It was necessary to perform these experiments on a *Rag2*$^{-/-}$ background due to an adaptive immune response to intramuscular lentiviral infection that appears to promote silencing of virally encoded genes. As expected, infection of *K-ras*$^{LSL\text{-}G12D}$*; Arf*$^{GFP/+}$*; Rag2*$^{-/-}$ mice with lentiviruses expressing only Cre failed to induce tumor formation, presumably due to the remaining functional allele of *Arf*. However, lentiviruses that contained Cre and an shRNA targeting both p19^{Arf} and p16^{Ink4a} generated sarcomas, demonstrating the efficiency of this knockdown system (Fig. S7).

Given the possible role of Snf5 in p19^{Arf} activation, we next tested if Snf5 depletion could promote sarcomagenesis in *K-ras*$^{LSL\text{-}G12D}$*; Arf*$^{GFP/+}$*; Rag2*$^{-/-}$ animals. Strikingly, Snf5 knockdown led to reproducible sarcoma formation with stable repression of Snf5 levels in the resulting tumors (Fig. 4 *C* and *E*). Histological analysis revealed very similar histopathologies between Snf5 knockdown tumors and those originating from control infections of *K-ras*$^{LSL\text{-}G12D}$*; Arf*$^{GFP/GFP}$*; Rag2*$^{-/-}$ animals. Both groups had tumors with areas of both large epithelioid cells and more spindle-shaped cells (Fig. 4*D*). Importantly, genomic PCR analysis showed retention of the wild-type allele of p19^{Arf}, indicating that there was no selective pressure to further inactivate the p19^{Arf}-p53 pathway during tumor progression (Fig. 4*E*). Together, these studies performed in vitro and in vivo suggest that Snf5 functions as a critical link between oncogenic K-ras expression and induction of the tumor suppressor pathway controlled by p19^{Arf}.

Discussion

The ability of oncogenic signaling to directly engage tumor suppressor pathways prevents the outgrowth of incipient tumor cells harboring initiating oncogenic mutations. Any variability in the nature or strength of any such tumor suppressor induction could have a profound influence on the potential tumorigenicity of mutated cells. Although a number of earlier studies have shown that oncogene levels play a critical role in determining whether cells become transformed or arrested, they have generally relied on experimentally manipulating the oncogene expression in a given cell type. In the present study, we identified naturally occurring variability in the degree of p19^{Arf} and p16^{Ink4a} induction following endogenous expression of K-ras^{G12D} in different cell types. Lung tumors display relatively low levels of these tumor suppressors, and this correlates with the ability of these cells to initiate the tumorigenic process with K-ras mutation alone. Introducing a *p19*^{Arf} mutant allele into these models moderately affects the tumor phenotype, and the loss of this pathway is still most likely a requisite event for development of advanced tumors (26). In contrast, sarcomas originating from K-ras^{G12D} mutant cells robustly up-regulate the *Ink4a/Arf* locus. This strong induction effectively blocks the transformation of K-ras^{G12D}–expressing muscle cells, such that the p19^{Arf}-p53 pathway must be completely abolished for tumor initiation to occur at all. Thus, it appears that resistance to oncogenic K-ras directly correlates with the strength of tumor suppressor induction.

One of the major determinants of oncogene-induced tumor suppression is thought to be the relative expression level of the oncogene. This does not appear to be the explanation for the cell-type–specific responses described here. A comparative analysis of K-ras expression as well as downstream signaling pathways failed to identify significant differences between lung tumors and sarcomas. Instead, we found that dynamic chromatin regulation plays an important role in tissue-specific *Ink4a/Arf* regulation. Specifically, we provide evidence that PcG proteins, including Bmi-1, repress this locus in lung tumors. By showing PcG-mediated regulation in established tumors, we build on previous work implicating Bmi-1 in

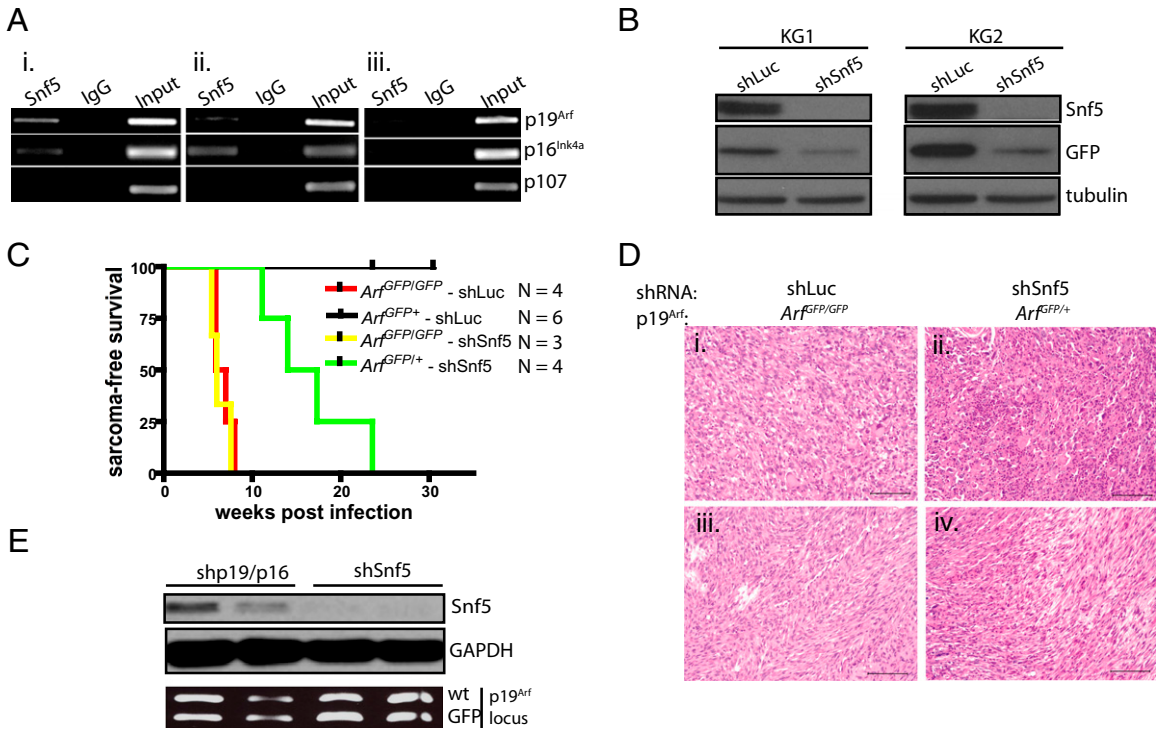

Fig. 4. The chromatin remodeler Snf5 contributes to the activation of $p19^{Arf}$ following oncogenic K-ras induction in the muscle. (*A*) Representative ChIP analysis of Snf5 on sarcoma-derived cell lines. (*i* and *ii*) Cell lines derived from *K-ras*$^{LSL\text{-}G12D}$*; Arf*$^{GFP/GFP}$ sarcomas induced with Ade-Cre infection. (*iii*) A cell line from a *K-ras*$^{LSL\text{-}G12D}$*; Arf*$^{GFP/GFP}$*; Rag2*$^{-/-}$ animal infected with a Cre-shSnf5 lentivirus. Snf5 enrichment at *Ink4a/Arf* is absent in the knockdown cell line. The p107 locus serves as a negative control for Snf5 binding. (*B*) Immunoblot analysis following in vitro knockdown of Snf5 in cell lines *i* and *ii* from *A*. (*C*) Kaplan–Meier graph of sarcoma-free survival for a cohort of *K-ras*$^{LSL\text{-}G12D}$*; Rag2*$^{-/-}$*; Arf*$^{GFP/+}$(black and green lines) or *Arf*$^{GFP/GFP}$ (red and yellow lines) mice infected intramuscularly with Cre-shLuc (red and black lines) or Cre-shSnf5 (yellow and green lines) lentiviruses. (*D*) Hematoxylin and eosin images of sarcomas from lenti-Cre; shLuc–infected *K-ras*$^{LSL\text{-}G12D}$*; Rag2*$^{-/-}$*; Arf*$^{GFP/GFP}$ (*i* and *iii*) or lenti-Cre; shSnf5–infected *K-ras*$^{LSL\text{-}G12D}$*; Rag2*$^{-/-}$*; Arf*$^{GFP/+}$ (*ii* and *iv*) animals. (*i* and *ii*) Regions containing circular epithelioid cells. (*iii* and *iv*) Regions composed of more spindle-shaped cells. (Scale bar: 100 μm.) (*E*) Western blot and genomic PCR analysis on a panel of sarcomas from *K-ras*$^{LSL\text{-}G12D}$*; Rag2*$^{-/-}$*; Arf*$^{GFP/+}$ animals derived from lentiviruses expressing Cre and hairpins to Snf5 or $p19^{Arf}$/$p16^{Ink4a}$.

control of lung tumor initiation (31). This regulation reduces the ability of affected cells to activate $p19^{Arf}$ and $p16^{Ink4a}$ in response to oncogenes and most likely contributes to the relative susceptibility of lung cells to transformation by $K\text{-}ras^{G12D}$.

The observation that sarcomas maintained some PcG-associated marks at *Ink4a/Arf* suggested that perhaps the initiating cell did repress the locus, but then further remodeled the local chromatin to allow for robust transcription in response to $K\text{-}ras^{G12D}$. Because SWI/SNF-remodeling complexes have been shown to be important for induction of PcG-regulated genes, we examined this class of genes as a possible link between oncogenic K-ras activation and Ink4a/Arf expression. Indeed, we identified Snf5 as an important mediator of oncogenic K-ras–dependent $p19^{Arf}$ induction in the muscle, implicating another chromatin-modifying complex in *Ink4a/Arf* regulation. At present, the relationship between oncogenic K-ras and Snf5 is unclear. Interestingly, K-ras knockdown can reduce Snf5 levels, suggesting that oncogenic signaling directly impinges on SWI/SNF function (Fig. S8). Nonetheless, because these chromatin-remodeling complexes mainly reposition nucleosomes, their role is largely to create a permissive environment for other transacting factors. Thus, oncogenic K-ras most likely also signals to transcriptional activators, and identifying these direct regulators is an important future direction. Of note, although several canonical inducers of *Ink4a/Arf*, such as E2F1, E2F3, and DMP1, were up-regulated in sarcomas (Fig. S9*A*), we were unable to functionally validate these genes in $p19^{Arf}$ up-regulation with our in vivo lentivirus system.

One current model to explain tissue-specific $p19^{Arf}$ induction presumes that under normal conditions PcG represses *Ink4a/Arf* in the cell-of-origin of both lung tumors and sarcomas. However, following oncogene activation, only lung tumors retain functional PcG repression. One possibility to account for this tissue-specific difference is that Snf5's main role in sarcomagenesis is to evict PcG from *Ink4a/Arf* in sarcomas, as it does in malignant rhabdoid tumors (30). It would appear that a similar effect does not occur in the cell-of-origin of lung tumors. Although the expression level of Snf5 is similar between the two tumor types (Fig. S9 *B* and *C*), it is still unclear whether tissue-specific activity or localization of SWI/SNF complexes could be the explanation for this difference. Another factor mediating PcG loss from chromatin is enhanced p38 MAPK activity (32, 33). However, we have been unable to observe differences in the activation status of this pathway between the two tumors types (Fig. S4).

An alternative model for the different levels of PcG regulation in the established tumors is that they represent the relative amount or activity state in the respective cells-of-origin. Having a lower degree of PcG-bound chromatin initially could reduce the requirements for gene activation in the muscle following oncogenic K-ras induction. Such a scenario has been proposed to explain the cell-type–specific requirements for $p19^{Arf}$ loss in the transformation of progenitor versus more differentiated B and T cells in the hematopoietic system, where PcG is thought to repress *Ink4a/Arf* mainly in stem cells (34). The precise identity of the respective cells-of-origin for lung tumors and sarcomas is currently unknown, thus precluding a meaningful analysis of PcG recruitment pre-K-ras activation.

Cell-type specificity in the activation threshold for the *Ink4a/Arf* locus might relate to the basal proliferative rate of the tissues in question. The lung epithelium constantly receives damage from irritants in the environment, thus requiring significant repair in

the form of cellular regeneration. To allow for this constant potential for repair, certain cells in the lung might stably silence $p19^{Arf}$ and $p16^{Ink4a}$ via PcG. In the context of oncogenic K-ras, the repression of this locus would allow cells to proliferate and form tumors. In contrast, muscles require minimal proliferative capacity and therefore might keep *Ink4a/Arf* in a chromatin state more conducive to potential activation. Consequently, if these cells acquire an oncogenic Ras mutation, they robustly induce $p19^{Arf}$ and $p16^{Ink4a}$ and effectively block tumor formation.

Lung tumors, as well as a variety of other epithelial cancers that originate from cells with a relatively high turnover rate, are much more common than soft-tissue sarcomas. The inherent differences in oncogene-induced tumor suppression across cell types could be the mechanistic basis for these observations. In addition, the fact that early lesions in some tissues have left key tumor suppressor pathways intact might have profound clinical implications if such anti-growth and pro-cell death pathways could be mobilized therapeutically.

Materials and Methods

Mice. Information on mouse strains is provided in the *SI Materials and Methods*. Virally induced lung tumors and sarcomas were generated as previously described (23, 24). Tamoxifen (Sigma) was dissolved in corn oil at 15 mg/mL and injected intraperitoneally every other day for 5 days. For lung tumor studies, *K-ras*^{LA2}; *Arf*^{GFP} compound mutant mice were killed at 6 or 12 weeks of age, and their lungs were processed as previously described (24). Bioquant Image Analysis was used to quantify tumor burden. Aged cohorts of *K-ras*^{LA2}; *Arf*^{GFP} mice as well as those used for virally induced sarcoma generation were monitored for visible masses or until they became moribund. Masses were processed similarly to the lungs. Animal studies were approved by Massachusetts Institute of Technology's Committee for Animal Care and conducted in compliance with Animal Welfare Act Regulations and other federal statutes relating to animals and experiments involving animals and adhered to the principles set forth in the 1996 National Research Council Guide for Care and Use of Laboratory Animals (institutional animal welfare assurance no. A-3125-01).

Lentiviral Vectors and shRNA Cloning. In vitro knockdown studies used a modified version of pSICO-Puro (35), Puro- sh2.0. The Cre-shRNA lentivirus for sarcoma formation was a gift from M. Kumar and K. Lane (Massachusetts Institute of Technology Koch Institute). Lung tumor formation in *K-ras*$^{FSF\text{-}G12D}$ relied on pSICO-Flpo. Target sequences for shRNA knockdown were identified using pSICO Oligomaker V 1.5 (A. Ventura, Memorial Sloan Kettering Cancer Center). Cloning of DNA oligos into the U6-shRNA cassette in the above vectors was done as described previously (35). Additional cloning details and shRNA sequences are described in *SI Materials and Methods*.

Lentivirus Production and Knockdown Studies. Lentiviral production was performed as described previously (36). For in vivo infections, viral pellets were resuspended in 1× HBSS, pH 7.4. A total of 50–100 μL was administered either intratracheally or intramuscularly.

Protein extraction/immunoblotting, mRNA isolation/quantitative PCR analysis, ChIP methods, and information about cell lines are provided in *SI Materials and Methods*.

ACKNOWLEDGMENTS. We are grateful to C. Sherr and F. Zindy for the *Arf*^{GFP} mice. We also thank D. Crowley for histological preparations; R. Bronson and C. Fletcher for histopathological analyses; P. Iaquinta, B. Berstein, M. Ku, and T. Thruong for technical assistance; M. DuPage for help with intratracheal infections; and D. Feldser and A. Cheung for critical reading of the manuscript. This work was supported in part by grant 5-U01-CA84306 from the National Institutes of Health and in part by Cancer Center Support (core) Grant P30-CA14051 from the National Cancer Institute. T.J. is a Howard Hughes Medical Institute Investigator and a Daniel K. Ludwig Scholar.

1. Lowe SW, Cepero E, Evan G (2004) Intrinsic tumour suppression. *Nature* 432:307–315.
2. Mooi WJ, Peeper DS (2006) Oncogene-induced cell senescence: Halting on the road to cancer. *N Engl J Med* 355:1037–1046.
3. Collado M, Serrano M (2006) The power and the promise of oncogene-induced senescence markers. *Nat Rev Cancer* 6:472–476.
4. Lowe SW, Sherr CJ (2003) Tumor suppression by Ink4a-Arf: Progress and puzzles. *Curr Opin Genet Dev* 13:77–83.
5. Serrano M, Lin AW, McCurrach ME, Beach D, Lowe SW (1997) Oncogenic ras provokes premature cell senescence associated with accumulation of p53 and p16INK4a. *Cell* 88:593–602.
6. Collado M, et al. (2005) Tumour biology: Senescence in premalignant tumours. *Nature* 436:642.
7. Palmero I, Pantoja C, Serrano M (1998) p19ARF links the tumour suppressor p53 to Ras. *Nature* 395:125–126.
8. Johnson L, et al. (2001) Somatic activation of the K-ras oncogene causes early onset lung cancer in mice. *Nature* 410:1111–1116.
9. Woods D, et al. (1997) Raf-induced proliferation or cell cycle arrest is determined by the level of Raf activity with arrest mediated by p21Cip1. *Mol Cell Biol* 17:5598–5611.
10. Tuveson DA, et al. (2004) Endogenous oncogenic K-ras(G12D) stimulates proliferation and widespread neoplastic and developmental defects. *Cancer Cell* 5:375–387.
11. Sarkisian CJ, et al. (2007) Dose-dependent oncogene-induced senescence in vivo and its evasion during mammary tumorigenesis. *Nat Cell Biol* 9:493–505.
12. Murphy DJ, et al. (2008) Distinct thresholds govern Myc's biological output in vivo. *Cancer Cell* 14:447–457.
13. Bracken AP, et al. (2007) The Polycomb group proteins bind throughout the INK4A-ARF locus and are disassociated in senescent cells. *Genes Dev* 21:525–530.
14. Chen H, et al. (2009) Polycomb protein Ezh2 regulates pancreatic beta-cell Ink4a/Arf expression and regeneration in diabetes mellitus. *Genes Dev* 23:975–985.
15. Dhawan S, Tschen SI, Bhushan A (2009) Bmi-1 regulates the Ink4a/Arf locus to control pancreatic beta-cell proliferation. *Genes Dev* 23:906–911.
16. Miyazaki M, et al. (2008) Thymocyte proliferation induced by pre-T cell receptor signaling is maintained through polycomb gene product Bmi-1-mediated Cdkn2a repression. *Immunity* 28:231–245.
17. Valk-Lingbeek ME, Bruggeman SW, van Lohuizen M (2004) Stem cells and cancer: The polycomb connection. *Cell* 118:409–418.
18. Volanakis EJ, Williams RT, Sherr CJ (2009) Stage-specific Arf tumor suppression in Notch1-induced T-cell acute lymphoblastic leukemia. *Blood* 114:4451–4459.
19. Williams RT, Sherr CJ (2007) The ARF tumor suppressor in acute leukemias: Insights from mouse models of Bcr-Abl-induced acute lymphoblastic leukemia. *Adv Exp Med Biol* 604:107–114.
20. Gebuhr TC, Bultman SJ, Magnuson T (2000) Pc-G/trx-G and the SWI/SNF connection: Developmental gene regulation through chromatin remodeling. *Genesis* 26:189–197.
21. Tamkun JW, et al. (1992) brahma: A regulator of Drosophila homeotic genes structurally related to the yeast transcriptional activator SNF2/SWI2. *Cell* 68:561–572.
22. Zindy F, et al. (2003) Arf tumor suppressor promoter monitors latent oncogenic signals in vivo. *Proc Natl Acad Sci USA* 100:15930–15935.
23. Kirsch DG, et al. (2007) A spatially and temporally restricted mouse model of soft tissue sarcoma. *Nat Med* 13:992–997.
24. Jackson EL, et al. (2001) Analysis of lung tumor initiation and progression using conditional expression of oncogenic K-ras. *Genes Dev* 15:3243–3248.
25. Stott FJ, et al. (1998) The alternative product from the human CDKN2A locus, p14(ARF), participates in a regulatory feedback loop with p53 and MDM2. *EMBO J* 17:5001–5014.
26. Jackson EL, et al. (2005) The differential effects of mutant p53 alleles on advanced murine lung cancer. *Cancer Res* 65:10280–10288.
27. Gil J, Peters G (2006) Regulation of the INK4b-ARF-INK4a tumour suppressor locus: All for one or one for all. *Nat Rev Mol Cell Biol* 7:667–677.
28. Ventura A, et al. (2007) Restoration of p53 function leads to tumour regression in vivo. *Nature* 445:661–665.
29. Raymond CS, Soriano P (2007) High-efficiency FLP and PhiC31 site-specific recombination in mammalian cells. *PLoS One* 2:e162.
30. Kia SK, Gorski MM, Giannakopoulos S, Verrijzer CP (2008) SWI/SNF mediates polycomb eviction and epigenetic reprogramming of the INK4b-ARF-INK4a locus. *Mol Cell Biol* 28:3457–3464.
31. Dovey JS, Zacharek SJ, Kim CF, Lees JA (2008) Bmi1 is critical for lung tumorigenesis and bronchioalveolar stem cell expansion. *Proc Natl Acad Sci USA* 105:11857–11862.
32. Wong ES, et al. (2009) p38MAPK controls expression of multiple cell cycle inhibitors and islet proliferation with advancing age. *Dev Cell* 17:142–149.
33. Voncken JW, et al. (2005) MAPKAP kinase 3pK phosphorylates and regulates chromatin association of the polycomb group protein Bmi1. *J Biol Chem* 280:5178–5187.
34. Williams RT, Sherr CJ (2008) The INK4-ARF (CDKN2A/B) locus in hematopoiesis and BCR-ABL-induced leukemias. *Cold Spring Harb Symp Quant Biol* 73:461–467.
35. Ventura A, et al. (2004) Cre-lox-regulated conditional RNA interference from transgenes. *Proc Natl Acad Sci USA* 101:10380–10385.
36. Rubinson DA, et al. (2003) A lentivirus-based system to functionally silence genes in primary mammalian cells, stem cells and transgenic mice by RNA interference. *Nat Genet* 33:401–406.

Supporting Information

Young and Jacks 10.1073/pnas.1004796107

SI Materials and Methods

Mice. *Arf*^{GFP} mice were provided by C. Sherr (St. Jude Children's Hospital, Memphis, TN), *Trp53*^{flox} were provided by A. Berns (The Netherlands Cancer Institute, Amsterdam, The Netherlands), and *Rag2*$^{-}$ mice were purchased from the Jackson Laboratory. *K-ras*^{LA2}, *K-ras*$^{LSL-G12D}$, *R26*^{CreER}, and *K-ras*$^{FSF-G12D}$ mice were generated in our laboratory. All animals were maintained on a mixed background comprising 129S4/SvJae and C57BL/6 strains.

Cell Lines and in Vitro Experiments. Cell lines were generated from sarcomas by mincing freshly extracted tissue with a razor blade followed by digesting with trypsin for 15 min at 37 °C. Dissociated tissue was resuspended in DMEM (10% FBS, 2 mM glutamine), and resulting cell lines were subsequently passaged in this media. For lentivirus experiments, target cells were selected in 5 μg/mL of puromyocin for 3 days following supernatant transfer. Cells were collected for analysis 2–4 days later. 293T cells for virus production were grown in DMEM.

Lentiviral Construction. To generate Puro-sh2.0, pSICO-Puro was digested with NotI and XhoI to remove the 3′ tata-lox and shRNA cloning site. The incompatible ends were blunted and subsequently ligated together. The resulting vector was digested with PstI and EcoRI to remove the U6 promoter-5′ tatalox segment and ligated to the U6 promoter-shRNA cloning site fragment from a PstI/EcoRI digest from the Cre-shRNA vector. pSICO-Flpo was generated by amplifying pgkFlpo from pgkFlpobpA (Addgene) with EcoRI and NotI sites engineered on the 5′ and 3′ ends, digesting with EcoRI/NotI, and ligating with a fragment of pSICO-GFP that had been digested previously to remove CMV-GFP. shRNA sequences are listed in Table S4.

Protein Extraction and Immunoblots. Cell lines were lysed in RIPA buffer (10 mM Tris, pH 7.5, 150 mM NaCl, 1 mM EDTA, 1% Tx-100, 0.1% SDS, 0.5% sodium deoxycholate, 1 mM DTT) plus mini complete protease inhibitors (Roche) and phosphatase inhibitors (mixtures 1 and 2) (Sigma) for 10 min on ice. Snap-frozen tissue was finely minced with a razor blade on ice in TNE buffer (50 mM Tris, pH 7.5, 150 mM NaCl, 2 mM EDTA, supplemented with 1% Tx-100, 0.1% SDS, 1 mM DTT, and the same protease and phosphatase inhibitors mentioned above) and then rotated for 15 min at 4 °C. Both in vitro and in vivo samples were centrifuged to remove insolubles and quantitated using a Bradford assay (Bio-Rad). Samples were then diluted in loading buffer, separated on 10–15% SDS–PAGE gels, transferred to PVDF membranes, and incubated with primary antibodies (Table S1). HRP-conjugated secondary antibodies were used in conjunction with ECL+ detection systems (Amersham). Levels of Ras-GTP were determined with the Ras activation kit (Millipore).

mRNA Isolation/Quantitative PCR Analysis. RNA was extracted either using an RNeasy kit along with Qiashredder columns (Qiagen) or using TRIzol (Invitrogen) according to the manufacturer's instructions. cDNA synthesis was performed on 1 μg of RNA using oligo(dT) primers and SuperScript III (Invitrogen). cDNAs were analyzed by quantitative PCR using Taqman detection systems in an ABI PRISM 7000 Sequence Detection System Thermo Cycler (Applied Biosystems) (Table S2). Relative mRNA levels were calculated using cycle threshold difference (ΔC_T) to control mRNA (TBP). In some instances, normal lung tissue served as an additional baseline ($\Delta\Delta C_T$ method).

PCR Analysis on Tumor DNA. DNA was prepared from tumors and subjected to standard PCR analysis. PCR primers were as follows: Arf-1—AGTACAGCAGCGGGAGCATGG; Arf-2—TTGAGGAGGACCGTGAAGCCG; and Neo-2—ACCACACTGCTCGACATTGGG.

Chromatin Immunoprecipitation. For the in vivo chromatin immunoprecipitation (ChIP), tumor tissue was cut up with razor blades in PBS, formaldehyde was added to 1%, and samples were incubated for 15 min at room temperature. Cross-linking was stopped by incubating with 0.125 M glycine for 5 min, samples were washed once with cold PBS, pellets were resuspended in cell lysis buffer [5 mM piperazine-N, N'-bis(2-ethanesulfonic acid) (Pipes), pH 8.0, 85 mM KCL, 0.5% Igepal], homogenized in a dounce homogenizer, and incubated at 4 °C for 10 min. After centrifugation, pellets were resuspended in nuclear lysis buffer (50 mM Tris, pH 8.1, 10 mM EDTA, 1% SDS) for 15 min on ice. Sonication was then done in a Branson 250 Sonifier to the appropriate shear length, debris was removed by centrifugation, and sheared chromatin was diluted 6× in dilution buffer (16.7 Tris, pH 8.1, 167 mM NaCl, 1.2 mM EDTA, 1.1% Tx-100, 0.01% SDS) before incubating with Protein A beads (Sigma) to preclear. Samples were evenly split for overnight immunoprecipitations with 1–3 μg of the appropriate antibodies: histone H3 trimethyl K27 (ab6002; Abcam), histone H3 trimethyl K4 (04-745-Millipore), acetylated histone H3 (06-599; Millipore), Bmi-1 (supernatant provided by J. Lees, Massachusetts Institute of Technology Koch Institute), and control IgGs (Santa Cruz Biotechnology). Inputs were taken from IgG samples before addition of Protein A beads the following day. Following incubation with beads for 1 h at 4 °C, beads were washed twice with a low-salt immune complex wash buffer (20 mM Tris, pH 8.1, 150 mM NaCl, 2mM EDTA, 1% Tx-100, 0.1% SDS), twice with lithium chloride (LiCl) immune complex wash buffer (10 mM Tris, pH 8.1, 1 mM EDTA, 1% Nonidet P-40, 1% Na deoxycholate, 0.25 M LiCl), and twice with 1× 10 mM Tris, 1 mM EDTA (TE), pH 8. DNA was eluted in 1× TE, 1% SDS, 150 mM NaCl, 5 mM DTT at 65 °C, and cross-links were reversed overnight at 65 °C. Proteinase K was added, and samples were incubated at 55 °C for 2 h before purifying DNA with Qiagen PCR purification columns.

For in vitro ChIP analyses, cells in 15-cm plates were fixed in 1% formaldehyde for 10 min at room temperature, followed by quenching in 0.125 M glycine. Samples were washed twice in ice-cold PBS and lysed directly in nuclear lysis buffer before continuing with the protocol above. Snf5 (A301-087A-1; Bethyl Laboratories) was used for the indicated IPs. Following purification, both IP and input DNA were subjected to standard PCR analysis with the primers indicated in Table S3.

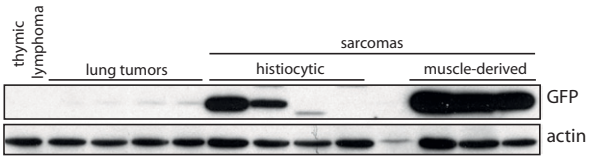

Fig. S1. Unique ArfGFP expression in different tumors from *K-ras*^{LA2}; *Arf*$^{GFP/GFP}$ mice. GFP Western blots on thymic lymphomas, lung tumors, histiocytic sarcomas, and muscle-derived sarcomas from *K-ras*^{LA2}; *Arf*$^{GFP/GFP}$ mice. In general, tumors that rely on p19^{Arf} loss display elevated levels of GFP, whereas those that form with K-ras mutation alone show very little expression.

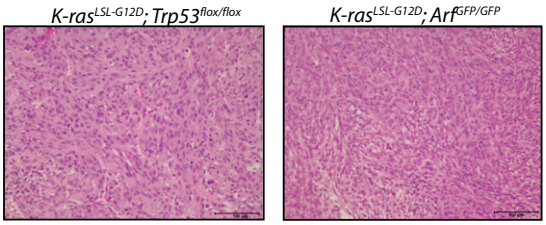

Fig. S2. *Arf*^{GFP} can substitute for *Trp53*^{flox} in K-ras^{G12D}–driven sarcomagenesis. Hematoxylin and eosin images showing similar histology of soft-tissue sarcomas generated by Ad-Cre infection of the hind limbs of *K-ras*$^{LSL-G12D}$; *Trp53*$^{flox/flox}$ (*Left*) or *K-ras*$^{LSL-G12D}$; *Arf*$^{GFP/GFP}$ (*Right*) animals. (Magnification: ×200; scale bar: 100 μm.)

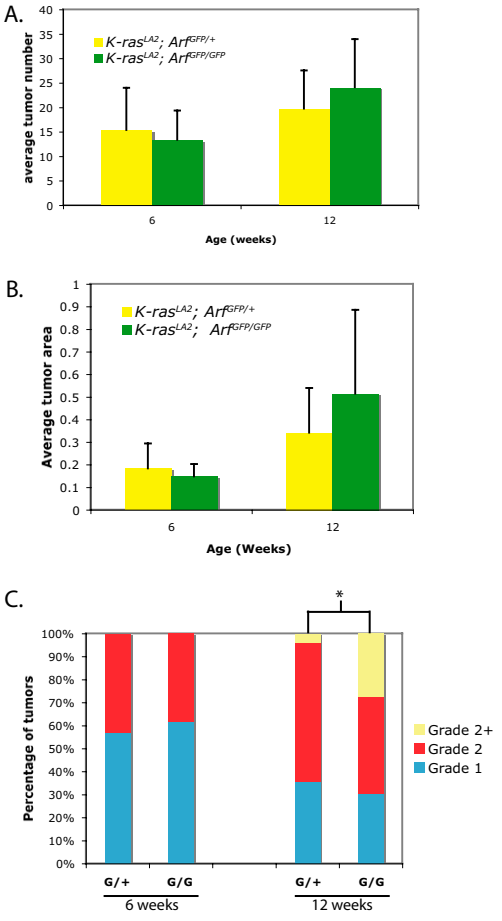

Fig. S3. Effects of p19^{Arf} deficiency on *K-ras*^{LA2} lung tumors. *K-ras*^{LA2}; *Arf*$^{GFP/+}$ (yellow bars, *A* and *B*) and *K-ras*^{LA2}; *Arf*$^{GFP/GFP}$ (green bars, *A* and *B*) littermates were aged either 6 or 12 weeks, at which point their lungs were processed for histological examination. One representative section per mouse was analyzed to calculate the average tumor number (*A*), the average tumor size (*B*), and each individual tumor's histopathological grade (*C*). (*C*) G/+: *K-ras*^{LA2}; *Arf*$^{GFP/+}$; G/G: *K-rasLA2; Arf*$^{GFP/GFP}$. (*A* and *B*) $P > 0.05$ for comparison between genotypes within one age group (Student's *t* test). (*C*) *$P < 0.001$ (Fisher's exact test). $n = 7$ (*Arf*$^{GFP/+}$ and *Arf*$^{GFP/GFP}$ at 6 weeks). $n = 12$ (*Arf*$^{GFP/+}$) and $n = 10$ (*Arf*$^{GFP/GFP}$) at 12 weeks. Error bars indicate SD.

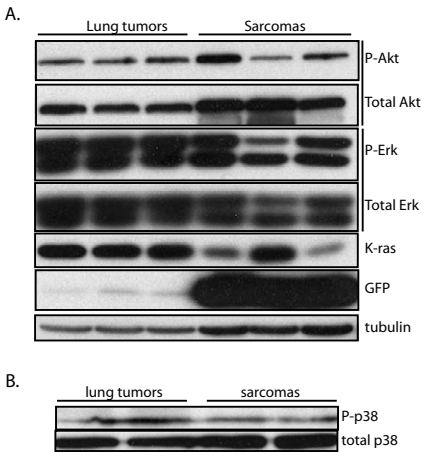

Fig. S4. Similar levels of oncogenic K-ras and downstream signaling pathways in lung tumors and sarcomas from *K-ras^{LA2}; Arf$^{GFP/GFP}$* mice. Western blot analysis of oncogenic signaling in three lung tumors and sarcomas from *K-ras^{LA2}; Arf$^{GFP/GFP}$* mice. MAPK (P-Erk) and PI3K (P-Akt) signaling pathways and total K-ras levels are shown in *A*, and *B* shows similar levels of p38MAPK signaling.

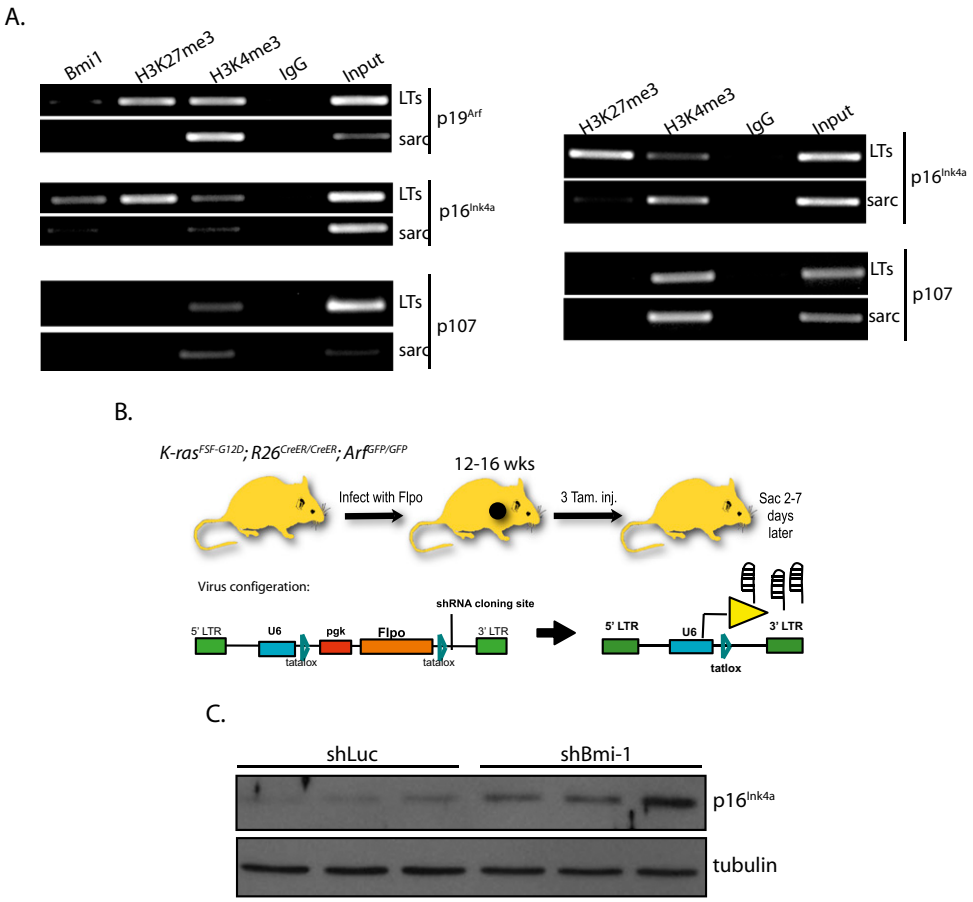

Fig. S5. Additional Polycomb group (PcG) analysis of *K-ras^{LA2}; Arf$^{GFP/GFP}$* lung tumors and sarcomas. (*A*) More examples of greater enrichment of a PcG-associated histone mark (H3K27me3) and Bmi-1 at *Ink4a/Arf* in lung tumors compared to sarcomas. H3-K4: trimethylated histone lysine 4 of histone H3, a mark of transcriptionally active promoters. (*B*) Schematic of inducible knockdown strategy. See *Results* section in main text, *PcG Proteins Actively Repress Ink4a/Arf in Established Lung Tumors,* for details. (*C*) Western blot analysis of p16^{Ink4a} in a panel of tumors from inducible shRNA (Luc or Bmi-1) experiments in vivo.

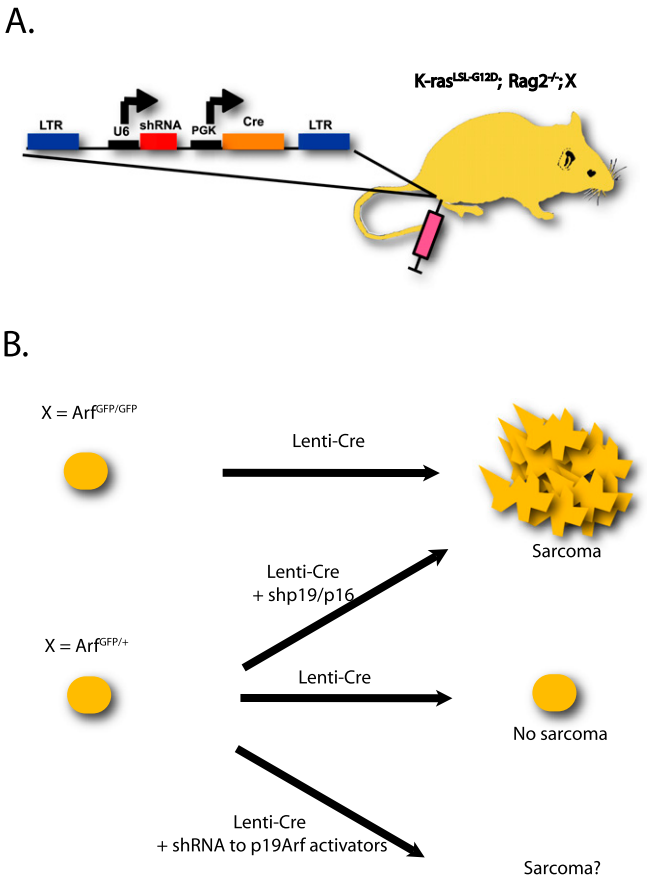

Fig. S6. Schematic of experimental design to identify functionally significant activators of p19^{Arf} during sarcomagenesis. (*A*) A bifunctional lentivirus expressing Cre and a shRNA is used to infect the muscles of *K-ras*$^{LSL-G12D}$*; Rag2*$^{-/-}$ mice that are either heterozygous (*Arf*$^{GFP/+}$) or homozygous null (*Arf*$^{GFP/GFP}$) for p19^{Arf}. (*B*) Sarcoma formation is completely inhibited by the presence of an activated, functional copy of p19^{Arf}. Therefore, sarcomas form only when infecting *Arf*$^{GFP/GFP}$ animals with Cre alone or when infecting *Arf*$^{GFP/+}$ mice with a shRNA to p19^{Arf}. Knockdown of critical activators of p19^{Arf} would possibly lead to sarcoma formation in *Arf*$^{GFP/+}$ mice as well.

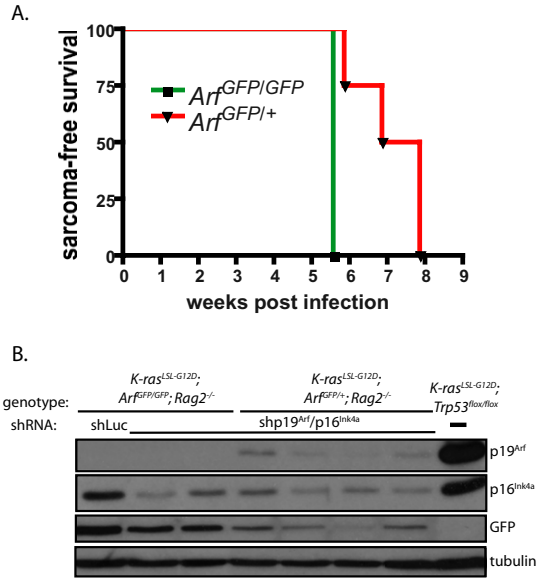

Fig. S7. Bifunctional lentiviruses containing Cre and shRNA to p19^{Arf}/p16^{Ink4a} efficiently generate sarcomas in *K-ras*$^{LSL-G12D}$*; Arf*$^{GFP/+}$*; Rag2*$^{-/-}$ animals. (*A*) Kaplan–Meier graph of sarcoma-free survival of *K-ras*$^{LSL-G12D}$*; Rag2*$^{-/-}$ mice that are either heterozygous (*Arf*$^{GFP/+}$: red line) or homozygous null (*Arf*$^{GFP/GFP}$: green line) for p19^{Arf}. Both groups of mice were infected intramuscularly with lentiviruses containing Cre and a shRNA to a shared exon of p19^{Arf} and p16^{Ink4a}. $n = 2$ for *Arf*$^{GFP/GFP}$ and $n = 4$ for *Arf*$^{GFP/+}$ (*B*) Western blot analysis of tumors from animals in *A* as well as a negative control for p19^{Arf} (*K-ras*^{G12D}*; Arf*$^{GFP/GFP}$*; Rag2*$^{-/-}$ sarcoma; leftmost lane) and a positive control for p19^{Arf} (*K-ras*^{G12D}*; Trp53*$^{flox/flox}$ sarcoma; right-most lane). The knockdown tumors show reduced levels of p19^{Arf} and p16^{Ink4a}.

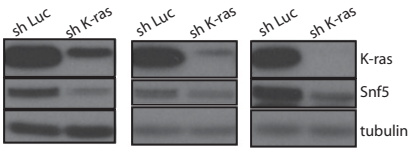

Fig. S8. K-ras knockdown decreases Snf5 levels in sarcoma cell lines. Western blot analysis showing efficient K-ras knockdown and decrease in Snf5 levels in three separate sarcoma cell lines.

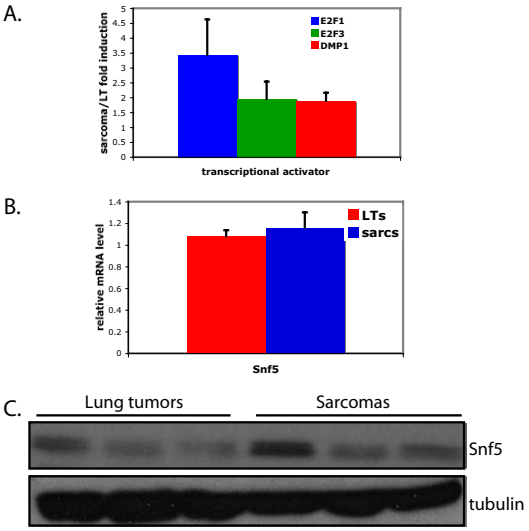

Fig. S9. Expression analysis of *Ink4a/Arf* activators in sarcomas and lung tumors. (*A*) qRT–PCR analysis of E2F1, E2F3, and DMP1 in *K-ras*^{LA2}; *Arf*$^{GFP/GFP}$ lung tumors and sarcomas. $n = 3$ for each tumor type, and $P < 0.05$ for expression difference between lung tumors and sarcomas. qRT–PCR (*B*) and immunoblot (*C*) analysis of Snf5 in lung tumors and sarcomas from *K-ras*^{LA2}; *Arf*$^{GFP/GFP}$ animals. In *B*, $n = 4$ for each tumor type. Error bars indicate SD.

Table S1. Antibodies used in Western blots

Antibody	Supplier	Catalog No.
β-Tubulin	Cell Signaling Technology	2146
Erk 1/2	Cell Signaling Technology	9102
phospho-Erk 1/2	Cell Signaling Technology	9101
Akt	Cell Signaling Technology	9272
Phospho-AktS473	Cell Signaling Technology	9271
β-actin	Santa Cruz Biotechnology	sc-1616
p16^{Ink4a}	Santa Cruz Biotechnology	sc-1207
p19^{Arf}	Santa Cruz Biotechnology	sc-32748
p27^{Kip}	Santa Cruz Biotechnology	sc-528
K-ras	Santa Cruz Biotechnology	sc-30
Snf5	Abcam	ab12167
Hsp90	BD Biosciences	610418
GAPDH	Chemicon International	MAB374
GFP	Novus Biologicals	NB 600–303

Table S2. Taqman probes for gene expression analysis

Gene	Taqman probe
E2F1	Mm00432936_m1
E2F3	Mm01138833_m1
Bmi-1	Mm00776122_gH
Ezh2	Mm00468449_m1
DMP1	Mm00516203_g1
Snf5	Mm00448776_m1
TBP	Mm00446973_m1

Table S3. Primers used for ChIP analysis

Locus	Forward primer	Reverse primer
$p19^{Arf}$	AAAGGGCGCAGCTACTGCTA	TCTTTGCTCCACGCCCATCT
$p16^{Ink4a}$	TTAGCGCTGTTTCAACGCCC	GCCACACTCTGCTCCTGACCT
p107	TTAGAGTCCGAGGTCCATCTTCT	GGGCTCGTCCTCGAACATATCC
cdc2	ACAGAGCTCAAGAGTCAGTTGGC	CGCCAATCCGATTGCACGTAGA

Table S4. shRNA sequences

Gene	Target sequence
Luciferase	GAGCTGTTTCTGAGGAGCC
$p19^{Arf}/p16^{Ink4a}$	GCTGGGTGGTCTTTGTGTA
Bmi-1	GTGATGACCTGGATTTGAA
Snf5	GGAAGAGGTGAATGATAAA
K-ras	GGAAACAAGTAGTAATTGA